

Mamba-CL: Optimizing Selective State Space Model in Null Space for Continual Learning

De Cheng^{1*}, Yue Lu^{2*}, Lingfeng He¹, Shizhou Zhang^{2†}, Xi Yang¹, Nannan Wang¹, Xinbo Gao³

¹ School of Telecommunications Engineering, Xidian University, China

² School of Computer Science, Northwestern Polytechnical University, China

³ Chongqing University of Posts and Telecommunications, China

Abstract

Continual Learning (CL) aims to equip AI models with the ability to learn a sequence of tasks over time, without forgetting previously learned knowledge. Recently, State Space Models (SSMs), particularly the Mamba model, have achieved notable success in computer vision. Building on the strengths of SSMs, this study explores leveraging the Mamba model for CL. Therefore, we introduce Mamba-CL, a framework that continuously fine-tunes the core SSMs of the large-scale Mamba foundation model by updating parameters orthogonal to the feature subspace of previous tasks. This approach theoretically guarantees the consistency objective aiming to preserve consistent output for each SSM module across both previous and current tasks, so as to overcome catastrophic forgetting issue. Specifically, we achieve this goal by deducing the overall consistency constraints on four key time-invariant parameters in the Mamba model, streamlining its recurrent state-space structure and non-linear discretization process in SSM. In practice, we apply the null-space projection to efficiently implement the orthogonality within Mamba model. Extensive experiments on four class-incremental benchmarks demonstrate the effectiveness of Mamba-CL for anti-forgetting, achieving superior performances to state-of-the-art methods. Code is available in the supplementary materials.

1. Introduction

Continual Learning (CL) aims to enable AI models to learn new tasks without forgetting previously acquired knowledge while processing sequentially arrived data, which is a capability essential for adapting to dynamic real-world environments. However, deep models face significant challenges in mitigating *catastrophic forgetting* when adapting to new data. This makes it difficult to achieve a balance be-

tween learning new knowledge and retaining prior knowledge, known as the *stability-plasticity dilemma*.

Existing CL methods can be broadly categorized into three types: *regularization-based* methods [18, 36, 42], *rehearsal-based* methods [1, 12, 43], and *network expansion* methods [5, 14, 41]. Among regularization-based approaches, subspace projection methods have gained attention for their promising performance in both convolutional neural networks (CNNs) [36] and vision transformers (ViTs) [24]. Specific methods such as OWM [42] and NSCL [36] have been effectively applied to CNNs, and VPT-NSP [24] has demonstrated strong performance for ViTs. Recently, State Space Models (SSMs) [9, 33], particularly the Mamba model [8], have achieved notable success in both sequence modeling and computer vision, with applications like De-focus Mamba [34] and VisionMamba [45]. Building on the strengths of SSMs in vision tasks, this study explores the potential of the Mamba model for CL through subspace projection.

To this end, we propose Mamba-CL, a method that fine-tunes the SSMs along a direction orthogonal to the subspace spanned by those features from previous tasks during training Mamba foundation model in a new task. By doing this, the interference with previously learned tasks can be minimized, thus effectively reducing *catastrophic forgetting* in CL. Although gradient orthogonal projections, which theoretically prevent forgetting, have been widely studied for CNNs, directly applying these methods to the Mamba structure introduces significant challenges due to: 1) the higher-order recurrent state-space structure, and 2) the non-linear discretization mechanism in SSMs. These factors make gradient orthogonal projection in SSMs considerably more complex than in CNNs, posing challenges for continual training of the Mamba-based foundation model.

Specifically, in the proposed Mamba-CL, we aim to continually fine-tune the core SSM blocks within the Mamba foundation model, by updating the parameters in the direction orthogonal to the subspace of input features from previous tasks. To achieve this, we analyze the objective that

*Equal contribution

†Corresponding author

keeps consistent outputs across tasks for SSM. As a result, by deducing sufficient conditions, we derive that the overall consistency objective can be satisfied via orthogonality constraints to four independent, time-invariant parameters in SSMs. The derived conditions provide a theoretical guarantee to prevent interference with previously learned knowledge through a gradient orthogonal projection mechanism, without catering to the higher-order recurrent state-space structure and non-linear discretization process in SSM.

In practice, we implement the derived sufficient *consistency conditions* by a null-space-based approximation solution [24, 36]. It enables efficient gradient orthogonal projections for the continual adaptation of the Mamba foundation model. Moreover, we introduce a balance factor to relax the orthogonality constraints so that we can make a good trade-off between stability and plasticity. We validate our Mamba-CL approach, which fine-tunes the Mamba foundation model with null-space projections, across several class-incremental benchmarks, including 10-split and 20-split ImageNet-R, 10-split CIFAR-100, and 10-split DomainNet. The proposed Mamba-CL demonstrates solid effectiveness in mitigating *catastrophic forgetting*, even in challenging long-sequence CL scenarios.

The main contributions can be summarized as follows:

- This is the first work to introduce orthogonal projection into the Mamba model for continual learning. The orthogonality constraint guarantees that the outputs of Mamba block remain consistent across tasks, thereby mitigating catastrophic forgetting.
- We theoretically derive four sufficient consistency conditions for the SSM block within the Mamba model. Based on these conditions, we introduce a null-space-based approximation to efficiently implement gradient orthogonal projections, enabling continual adaptation of the Mamba foundation model.
- Extensive experimental results demonstrate the effectiveness of our approach in anti-forgetting on four class-incremental benchmarks with diverse experimental settings, and our approach achieves superior performances to state-of-the-art methods.

2. Related Works

2.1. State Space Models (SSMs)

State Space Models (SSMs) are proposed to model the long-range dependencies [9, 33] in Natural Language Processing (NLP). [9] first introduces a Structured State-Space Sequence (S4) model based on the control theory, outperforming previous models in accuracy and speed. Mamba [8] proposes a data-dependent SSM block and designs a generic language model for various NLP tasks. Recently, the SSM structure has been investigated in computer vision tasks. Several attempts [15, 25, 35] design SSM-based vision

models for various vision tasks, such as video understanding and biomedical image segmentation. VisionMamba [45] first proposes a vision backbone consisting of bidirectional Mamba blocks, which achieves superior performance and memory efficiency over vision transformers. VMamba [23] further proposes Visual State-Space blocks and a 2D Selective Scan module based on the SSM to efficiently gather context for images. De-focus Mamba [34] devises bandpass filters and enhances training strategies to broaden the attention range, further improving the performance of the SSM-based model in vision tasks. Despite the difference in the design of visual Mamba blocks among existing models, they all rely on the SSM for context modeling. Inspired by the advancement of SSM models in vision tasks, this study seeks to harness the potential of SSM for CL.

2.2. Parameter-Regularization-based Continual Learning

A series of CNN-based methods [4, 18, 42] design various parameter regularization theories to mitigate catastrophic forgetting. Subspace projection methods [21, 31, 36, 42] propose to update parameters in the subspace orthogonal to the previous feature space. Through the orthogonality, the features from old tasks can remain unchanged after learning new tasks, thereby theoretically enhancing the stability of models. Recently, prompt-tuning-based CL methods [7, 32, 38, 39] utilizing pre-trained ViTs have achieved remarkable performance, where a small number of learnable prompts are introduced for the adaptation to downstream tasks. PGP [28] first proposes to update the visual prompts in the direction orthogonal to the previous input feature subspace. VPT-NSP [24] theoretically deduces two sufficient consistency conditions to strictly satisfy the orthogonality for prompt tuning, where the null space method [36] is utilized to implement the conditions. Inspired by these methods, we also adopt the null space approach [36] to construct the orthogonal projectors.

However, due to the higher-order recurrent state-space structure and the non-linear discretization operation in the SSM, the orthogonality constraints of the above methods are inapplicable to the Mamba architecture. We aim to deduce the consistency conditions for the SSMs and design dedicated projectors to implement the orthogonal projection, as introduced in the next section.

3. Preliminaries

Problem Definition. In continual learning, there is a sequence of tasks with non-overlapping classes. We define the task sequence as $\mathcal{T} = \{\mathcal{T}_1, \dots, \mathcal{T}_T\}$. $\mathcal{D}_t = \{\mathbf{x}_t^{<i>, y_t^{<i>} \}_{i=1}^{|\mathcal{T}_t|}$ is the dataset associated with the t -th task of size $|\mathcal{T}_t|$, where $\mathbf{x}_t^{<i> \in \mathbb{R}^{H \times W \times C}$ are training images and $y_t^{<i> \in \mathcal{Y}^t$ are ground-truth labels. \mathcal{Y}^t is the label

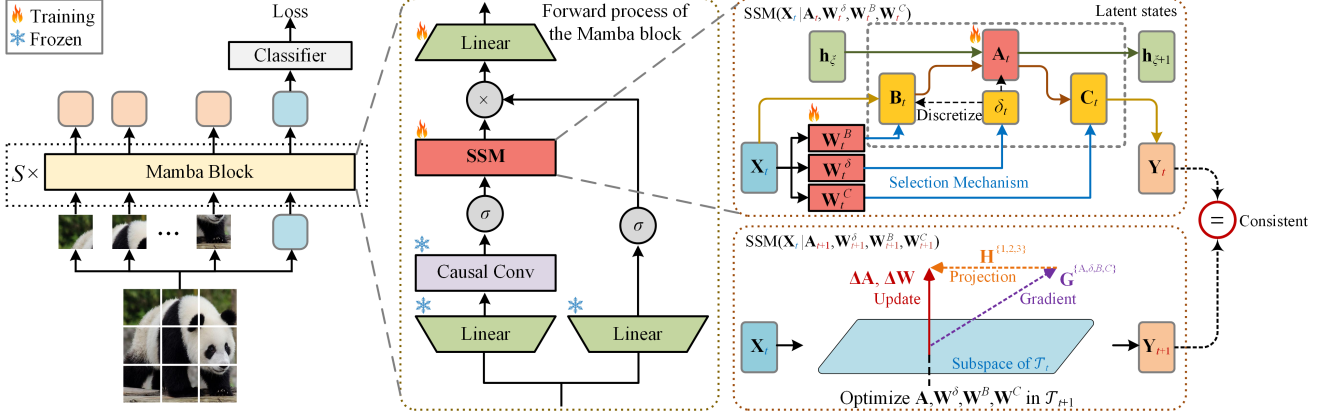


Figure 1. Illustration of the proposed Mamba-CL. The backbone contains S Mamba blocks. For each Mamba block, we fine-tune the weights \mathbf{W}^δ , \mathbf{W}^B , \mathbf{W}^C and \mathbf{A} within the SSM (as well as the linear layer after the SSM). To minimize forgetting, we aim to utilize orthogonal projections to keep the output unchanged from SSM after training the $t + 1$ -th task.

space of the t -th task, and $\mathcal{Y}^t \cap \mathcal{Y}^{t'} = \emptyset$ for $t \neq t'$ in class-incremental learning. The objective of continual learning is to train a model $f(\cdot|\theta)$ with parameters θ sequentially on T tasks and perform well on all seen classes $\mathcal{Y}^1 \cup \dots \cup \mathcal{Y}^T$.

Inspired by existing fine-tuning-based CL methods [24, 38, 39], we utilize a pre-trained De-focus Mamba [34] as our backbone. As illustrated in Fig.1, Mamba-CL tunes the parameters within the SSM blocks and the linear projections after the SSM blocks via orthogonal projection-based optimization, while maintaining others frozen.

3.1. The Forward Process of State Space Models

In this section, we outline the forward process of the State Space Model (SSM) in Mamba. Let $\mathbf{X} \in \mathbb{R}^{L \times D}$ denote an input sequence of SSM with token length L , where D represents the dimension of each token. The SSM requires four input parameters, including an input-invariant parameter \mathbf{A} , and three input-conditioned parameters \mathbf{B} , \mathbf{C} and δ [8]. First, the input \mathbf{X} undergoes three projection layers $s_B(\cdot)$, $s_C(\cdot)$ and $s_\delta(\cdot)$ to derive the above three input-conditioned parameters:

$$\begin{cases} \mathbf{B} = s_B(\mathbf{X}; \mathbf{W}^B) \in \mathbb{R}^{L \times N}, \\ \mathbf{C} = s_C(\mathbf{X}; \mathbf{W}^C) \in \mathbb{R}^{L \times N}, \\ \delta = \tau_\delta(\text{param} + s_\delta(\mathbf{X}; \mathbf{W}^\delta)) \in \mathbb{R}^{L \times 1}, \end{cases} \quad (1)$$

where $\mathbf{W}^B \in \mathbb{R}^{D \times N}$, $\mathbf{W}^C \in \mathbb{R}^{D \times N}$ and $\mathbf{W}^\delta \in \mathbb{R}^{D \times 1}$ denote the learnable weights in $s_B(\cdot)$, $s_C(\cdot)$ and $s_\delta(\cdot)$, respectively. Here, N denotes the dimension of each latent state in SSM. param is a bias term and $\tau_\delta(\cdot)$ denotes the soft-plus operation [8] to avoid negative values in δ . After that, the SSM transforms the ‘continuous parameters’ $(\mathbf{A}, \mathbf{B}, \delta)$ to ‘discrete parameters’ $(\bar{\mathbf{A}}, \bar{\mathbf{B}})$ through the zero-order hold (ZOH) discretization rule:

$$\begin{cases} \bar{\mathbf{A}} = \exp(\delta \mathbf{A}) \in \mathbb{R}^{L \times D \times N}, \\ \bar{\mathbf{B}} = (\delta \mathbf{A})^{-1} (\exp(\delta \mathbf{A}) - \mathbf{I}) \delta \mathbf{B} \in \mathbb{R}^{L \times D \times N}. \end{cases} \quad (2)$$

After that, the final output is derived through a global convolution with kernel $\bar{\mathbf{K}}$, and the convolutional kernel is constructed on top of the above parameters $\bar{\mathbf{A}}$, $\bar{\mathbf{B}}$ and \mathbf{C} . The forward process is formulated as follows:

$$\bar{\mathbf{K}} = \left[\mathbf{C}\bar{\mathbf{B}}, \mathbf{C}\bar{\mathbf{A}}\bar{\mathbf{B}}, \dots, \mathbf{C}\bar{\mathbf{A}}^k \bar{\mathbf{B}}, \dots \right], \quad (3)$$

$$\mathbf{Y} = \text{SSM}(\mathbf{X}|\mathbf{A}, \mathbf{W}^B, \mathbf{W}^C, \mathbf{W}^\delta) = \mathbf{X} * \bar{\mathbf{K}}, \quad (4)$$

where k denotes the kernel tensor corresponding to the k -th latent state within the SSM and \mathbf{Y} denotes the output of the SSM model. ‘*’ denotes the convolution operation. The learnable parameters in the SSM including $\mathbf{A} \in \mathbb{R}^{D \times N}$ and the projection weights $\mathbf{W}^{\{B,C,\delta\}} \in \mathbb{R}^{D \times \{N,N,1\}}$. Finally, the output \mathbf{Y} is fed into the next layer.

3.2. Orthogonal Projection in Convolutional Layers

For a convolutional layer $f_{\text{conv}}(\cdot|\Theta_t)$ after training the t -th task, we define its unrolled convolutional matrix as $\Theta_t \in \mathbb{R}^{D_{in} \times D_{out}}$, where D_{in} denotes the number of pixels in each kernel and D_{out} denotes the number of channels. We define a flattened input from the t -th task as $\mathbf{X}_t \in \mathbb{R}^{N \times D_{in}}$ with N patches. The forward process is simply formulated as a linear operation, where $f_{\text{conv}}(\mathbf{X}_t|\Theta_t) = \mathbf{X}_t \Theta_t$. The *orthogonal projection* aims to keep the output unchanged from the convolutional weight after training $t + 1$ -th task to minimize forgetting, which is formulated as follows:

$$f_{\text{conv}}(\mathbf{X}_t|\Theta_t) = f_{\text{conv}}(\mathbf{X}_t|\Theta_{t+1}), \quad (5)$$

where $\Theta_{t+1} = \Theta_t + \Delta\Theta$. $\Delta\Theta$ denotes the change of Θ before and after learning the $t + 1$ -th task. Then we derive the updating rule to achieve Eq.5:

$$\mathbf{X}_t \Theta_t = \mathbf{X}_t (\Theta_t + \Delta \Theta) \Rightarrow \mathbf{X}_t \Delta \Theta = \mathbf{0}. \quad (6)$$

The above term suggests that if the change of convolutional weight $\Delta \Theta$ in the new task is orthogonal to the previous input feature space \mathbf{X}_t , the output of old task instances will remain unchanged. Existing methods [21, 31, 36] implement Eq.6 by projecting the original gradient \mathbf{G}^Θ onto the orthogonal space of previous feature space through a projector $\mathbf{P} \in \mathbb{R}^{D_{in} \times D_{in}}$, where $\Delta \Theta = \mathbf{P} \mathbf{G}^\Theta$.

Similarly, for the SSM model with learnable parameters $\{\mathbf{A}, \mathbf{W}^B, \mathbf{W}^C, \mathbf{W}^\delta\}$, we also aim to remain the previous output unchanged while learning the new task:

$$\begin{aligned} SSM(\mathbf{X}_t | \mathbf{A}_t, \mathbf{W}_t^B, \mathbf{W}_t^C, \mathbf{W}_t^\delta) = \\ SSM(\mathbf{X}_t | \mathbf{A}_{t+1}, \mathbf{W}_{t+1}^B, \mathbf{W}_{t+1}^C, \mathbf{W}_{t+1}^\delta), \end{aligned} \quad (7)$$

where the subscripts t and $t+1$ denote the parameters trained after the t -th and $t+1$ -th tasks, respectively. Due to the complex forward propagation in SSM, the simple consistency condition given by Eq.6 is insufficient to achieve the above consistency term. In the next section, we will deduce the conditions to achieve Eq.7 in the SSM.

4. Methodology

In this section, we aim to deduce one or more conditions expressed in terms of the change of parameters to satisfy Eq.7. We use $\{\Delta \mathbf{A}, \Delta \mathbf{W}^B, \Delta \mathbf{W}^C, \Delta \mathbf{W}^\delta\}$ to denote the change of parameters before and after learning $t+1$ -th task.

4.1. Analysis of the Consistency Conditions

As shown in Fig.1, the output is determined by the global convolution in Eq.4. Therefore, to achieve Eq.7, the previous output from Eq.4 should be unchanged before and after learning the new task. We substitute Eq.4 into Eq.7:

$$\mathbf{X}_t * \bar{\mathbf{K}}_t = \mathbf{X}_t * \bar{\mathbf{K}}_{t+1}. \quad (8)$$

To achieve the consistency condition formulated in the above term, we derive the following equation:

$$\bar{\mathbf{K}}_t = \bar{\mathbf{K}}_{t+1}. \quad (9)$$

Through the definition of $\bar{\mathbf{K}}$ in Eq.3, the above consistency term can be transformed as follows:

$$\begin{aligned} \left[\mathbf{C}_t \bar{\mathbf{B}}_t, \dots, \mathbf{C}_t \bar{\mathbf{A}}_t^k \bar{\mathbf{B}}_t, \dots \right] = \\ \left[\mathbf{C}_{t+1} \bar{\mathbf{B}}_{t+1}, \dots, \mathbf{C}_{t+1} \bar{\mathbf{A}}_{t+1}^k \bar{\mathbf{B}}_{t+1}, \dots \right]. \end{aligned} \quad (10)$$

Since Eq.10 contains three variables, (*i.e.*, $\bar{\mathbf{A}}$, $\bar{\mathbf{B}}$ and \mathbf{C}), we analyze the sufficient conditions for which Eq.10 holds as a particular solution to the equation:

$$\begin{cases} \bar{\mathbf{A}}_t^k = \bar{\mathbf{A}}_{t+1}^k, \\ \bar{\mathbf{B}}_t = \bar{\mathbf{B}}_{t+1}, \\ \mathbf{C}_t = \mathbf{C}_{t+1}. \end{cases} \quad (11)$$

Next, we separately analyze the conditions under which the above consistency equations can be satisfied.

Analysis of the condition to satisfy $\bar{\mathbf{A}}_t^k = \bar{\mathbf{A}}_{t+1}^k$. According to the definition $\bar{\mathbf{A}} = \exp(\delta \mathbf{A})$ in Eq.2, we aim to deduce the conditions for the two variables \mathbf{A} and δ . Based on the definition of $\bar{\mathbf{A}}$, we first transform the condition $\bar{\mathbf{A}}_t = \bar{\mathbf{A}}_{t+1}$ as follows:

$$[\exp(\delta_t \mathbf{A}_t)]^k = [\exp(\delta_{t+1} \mathbf{A}_{t+1})]^k. \quad (12)$$

Since the exponential operation is element-wise, and given the monotonic increasing property of $[\exp(x)]^k$, the above term can be transformed as follows:

$$\delta_t \mathbf{A}_t = \delta_{t+1} \mathbf{A}_{t+1}. \quad (13)$$

As there are two potential variables (*i.e.*, $\Delta \delta$ and $\Delta \mathbf{A}$) in the single equation Eq.13, it is difficult to solve it directly. Given that δ is a discretization parameter that affects both \mathbf{A} and \mathbf{B} , we first keep $\delta_t = \delta_{t+1}$ so that the discretization process remains consistent. Base on that, we can decompose Eq.13 into two consistency conditions for δ and \mathbf{A} :

$$\begin{cases} \delta_t = \delta_{t+1}, \\ \delta_t \mathbf{A}_t = \delta_t \mathbf{A}_{t+1} = \delta_t (\mathbf{A}_t + \Delta \mathbf{A}) \Rightarrow \delta_t \Delta \mathbf{A} = \mathbf{0}. \end{cases} \quad (14)$$

To achieve $\delta_t = \delta_{t+1}$, given the definition $\delta = \tau_\delta(\text{param} + s_\delta(\mathbf{X}; \mathbf{W}^\delta))$ in Eq.1, we aim to obtain the consistency conditions for \mathbf{W}^δ . Since the softplus function τ_δ is monotonically increasing, and given $s_\delta(\mathbf{X}; \mathbf{W}^\delta) = \mathbf{X} \mathbf{W}^\delta$, the upper formula in Eq.14 can be simplified as follows:

$$\mathbf{X}_t \mathbf{W}_t^\delta = \mathbf{X}_t \mathbf{W}_{t+1}^\delta \Rightarrow \mathbf{X}_t \mathbf{W}_t^\delta = \mathbf{X}_t (\mathbf{W}_t^\delta + \Delta \mathbf{W}^\delta). \quad (15)$$

In this way, we derive the consistency condition for $\Delta \mathbf{W}^\delta$:

$$\mathbf{X}_t \Delta \mathbf{W}^\delta = \mathbf{0}. \quad (16)$$

By combining Eq.14 and Eq.16, we obtain two sufficient conditions of $\Delta \mathbf{A}$ and $\Delta \mathbf{W}^\delta$ for maintaining the consistency term $\bar{\mathbf{A}}_t^k = \bar{\mathbf{A}}_{t+1}^k$:

$$\begin{cases} \delta_t \Delta \mathbf{A} = \mathbf{0}, \\ \mathbf{X}_t \Delta \mathbf{W}^\delta = \mathbf{0}. \end{cases} \quad (17)$$

Analysis of the condition to satisfy $\bar{\mathbf{B}}_t = \bar{\mathbf{B}}_{t+1}$. According to the definition $\bar{\mathbf{B}} = (\delta \mathbf{A})^{-1} (\exp(\delta \mathbf{A} - \mathbf{I})) \delta \mathbf{B}$ in Eq.2, we formulate the consistency term in Eq.11 as follows:

$$\begin{aligned} (\delta_t \mathbf{A}_t)^{-1} (\exp(\delta_t \mathbf{A}_t - \mathbf{I})) \delta_t \mathbf{B}_t = \\ (\delta_{t+1} \mathbf{A}_{t+1})^{-1} (\exp(\delta_{t+1} \mathbf{A}_{t+1} - \mathbf{I})) \delta_{t+1} \mathbf{B}_{t+1}. \end{aligned} \quad (18)$$

Considering the deduced condition $\delta_t \mathbf{A}_t = \delta_{t+1} \mathbf{A}_{t+1}$ given by Eq.13, the above term can be simplified as follows:

$$\delta_t \mathbf{B}_t = \delta_{t+1} \mathbf{B}_{t+1}. \quad (19)$$

Given $\mathbf{B} = \mathbf{X}\mathbf{W}^B$ is the output of the projection layer $s_B(\cdot)$, the above equation can be expanded as:

$$\delta_t \mathbf{X}_t \mathbf{W}_t^B = \delta_{t+1} \mathbf{X}_t (\mathbf{W}_t^B + \Delta \mathbf{W}^B). \quad (20)$$

Considering the condition $\delta_t = \delta_{t+1}$ given by Eq.14 for parameter δ , we can derive the consistency condition for $\Delta \mathbf{W}^B$ by expanding the above equation:

$$\delta_t \mathbf{X}_t \Delta \mathbf{W}^B = \mathbf{0}. \quad (21)$$

Analysis of the condition to satisfy $\mathbf{C}_t = \mathbf{C}_{t+1}$. Given the definition of \mathbf{C} in Eq.1, where $\mathbf{C} = s_C(\mathbf{X}; \mathbf{W}^C)$, we reformulate $\mathbf{C}_t = \mathbf{C}_{t+1}$ as follows:

$$s_C(\mathbf{X}_t; \mathbf{W}_t^C) = s_C(\mathbf{X}_t; \mathbf{W}_{t+1}^C). \quad (22)$$

Given the linear operation in the projection layer $s_C(\cdot)$, where $s_C(\mathbf{X}; \mathbf{W}^C) = \mathbf{X}\mathbf{W}^C$, the consistency condition for $\Delta \mathbf{W}^C$ can be similarly derived:

$$\mathbf{X}_t \Delta \mathbf{W}^C = \mathbf{0}. \quad (23)$$

By combining Eq.17, Eq.21 and Eq.23, we derive four sufficient consistency conditions to satisfy Eq.7 for four updating parameters $\{\mathbf{A}, \mathbf{W}^B, \mathbf{W}^C, \mathbf{W}^\delta\}$:

$$\begin{cases} \delta_t \Delta \mathbf{A} = \mathbf{0}, \\ \mathbf{X}_t \Delta \mathbf{W}^\delta = \mathbf{0}, \\ \delta_t \mathbf{X}_t \Delta \mathbf{W}^B = \mathbf{0}, \\ \mathbf{X}_t \Delta \mathbf{W}^C = \mathbf{0}. \end{cases} \quad (24)$$

The above four conditions can achieve the consistency objective formulated in Eq.7 to minimize catastrophic forgetting of old knowledge. In the next section, we will describe the optimization process for updating the parameters under the above conditions in detail.

4.2. Optimization of Consistency Conditions

To jointly optimize these four conditions, we aim to solve the update of parameters $\{\Delta \mathbf{A}, \Delta \mathbf{W}^B, \Delta \mathbf{W}^C, \Delta \mathbf{W}^\delta\}$ to satisfy all conditions concurrently. Firstly, the optimization should make $\Delta \mathbf{W}^\delta$ and $\Delta \mathbf{W}^C$ orthogonal to the feature space spanned by \mathbf{X}_t . Subsequently, it should guarantee that $\Delta \mathbf{A}$ and $\Delta \mathbf{W}^B$ are orthogonal to the space spanned by δ_t and $\delta_t \mathbf{X}_t$ under the condition $\delta_t = \delta_{t+1}$.

Specifically, we utilize $\mathbf{G}^{\{A,B,C,\delta\}}$ to represent the gradient of the parameters generated by the optimizer. We aim to find a group of projectors $\mathbf{P}^{\{A,B,C,\delta\}}$ to project these gradients onto the orthogonal space of the aforementioned feature space to satisfy Eq.24:

$$\begin{cases} \Delta \mathbf{A} = \mathbf{P}^A \mathbf{G}^A, \\ \Delta \mathbf{W}^{\{B,C,\delta\}} = \mathbf{P}^{\{B,C,\delta\}} \mathbf{G}^{\{B,C,\delta\}}. \end{cases} \quad (25)$$

Inspired by the null-space optimization methods [24, 31, 36], the bases of the projection matrices \mathbf{P}^δ and \mathbf{P}^C should reside in the null space of \mathbf{X}_t . Meanwhile, the

bases of \mathbf{P}^A and \mathbf{P}^B should lie in the null space of δ_t and $\delta_t \mathbf{X}_t$. To obtain the null space bases, after training the t -th task, we extract the feature matrices $\bar{\mathbf{X}}_t, \bar{\delta}_t, \bar{\delta}_t \bar{\mathbf{X}}_t$ of all images from the t -th task. For example, $\bar{\mathbf{X}}_t = [\mathbf{X}_t^1, \dots, \mathbf{X}_t^m, \dots, \mathbf{X}_t^M] \in \mathbf{R}^{ML \times D}$ is built by the entire t -th dataset. \mathbf{X}_t^m is the feature of the m -th data point, and M is the number of data points. Then we derive the uncentered covariance matrices of the feature matrices, where $\mathbf{Q}_1 = \bar{\mathbf{X}}_t^\top \bar{\mathbf{X}}_t$, $\mathbf{Q}_2 = \bar{\delta}_t^\top \bar{\delta}_t$, and $\mathbf{Q}_3 = \bar{\delta}_t \bar{\mathbf{X}}_t^\top \bar{\delta}_t \bar{\mathbf{X}}_t$. The null space bases $\mathbf{U}_{1,0}$, $\mathbf{U}_{2,0}$ and $\mathbf{U}_{3,0}$ are obtained from the right singular vectors corresponding to the zero singular values through singular value decomposition (SVD) of $\{\mathbf{Q}_1, \mathbf{Q}_2, \mathbf{Q}_3\}$. Each group of null space bases constructs a subspace orthogonal to the corresponding feature subspace.

Note that since zero singular values do not always exist, we use an adaptive method to select the singular values close to zero as approximated zero singular values. Based on the observation that the singular values in descending order form an "L" shape [24], we first find the index of the corner point by calculating the maximum second derivative of the points: $R = J - \arg \max_j \{\lambda_{j-1} - 2\lambda_j + \lambda_{j+1}\}_{j=2}^{J-1}$, where J , R and λ_j denote the total number of singular values, the number of approximated zero singular values and the j -th singular value, respectively. Those right singular values corresponding to the R smallest singular values obtained by SVD are selected as the null space bases.

As a result, we derive the projectors $\mathbf{H}_1 = \mathbf{U}_{1,0} \mathbf{U}_{1,0}^\top$, $\mathbf{H}_2 = \mathbf{U}_{2,0} \mathbf{U}_{2,0}^\top$, and $\mathbf{H}_3 = \mathbf{U}_{3,0} \mathbf{U}_{3,0}^\top$ to enable that the parameter updates satisfy the conditions in Eq.24:

$$\begin{cases} \Delta \mathbf{W}^\delta = \mathbf{H}_1 \mathbf{G}^\delta, \\ \Delta \mathbf{W}^C = \mathbf{H}_1 \mathbf{G}^C, \\ \Delta \mathbf{A} = \mathbf{H}_2 \mathbf{G}^A, \\ \Delta \mathbf{W}^B = \mathbf{H}_3 \mathbf{G}^B. \end{cases} \quad (26)$$

To sum up, we use Eq.26 to perform orthogonal projections for parameter updating. The whole training process is outlined in Appendix A. To further balance the stability and plasticity of the model, we introduce a balance hyperparameter $\eta \in [0, 1]$ to relax the orthogonality constraints. For example, for $\Delta \mathbf{W}^\delta$, we combine the null space projection \mathbf{H}_1 and the identity matrix \mathbf{I} to derive a new projector $\bar{\mathbf{H}}_1$ for enhancing plasticity: $\bar{\mathbf{H}}_1 = \eta \mathbf{H}_1 + (1 - \eta) \mathbf{I}$. η represents the strictness degree of the orthogonality. After that, the updating rule of \mathbf{W}^δ is given by: $\Delta \mathbf{W}^\delta = \bar{\mathbf{H}}_1 \mathbf{G}^\delta$. Such a strategy can be applied to other parameters similarly to improve the model's plasticity.

5. Experiments

5.1. Experimental Setups

We mainly evaluate our approach across four class-incremental learning (CIL) benchmarks: 10-split and 20-

Table 1. Comparison between the proposed approach (Mamba-CL) and the baseline of sequential fine-tuning Mamba (Mamba-Seq). The upper bound means jointly training all the classes in the dataset. The value after \pm indicates the standard deviation.

| Method | 10-split ImageNet-R | | 20-split ImageNet-R | | 10-split CIFAR-100 | | 10-split DomainNet | |
|-------------|-------------------------|-------------------------|-------------------------|-------------------------|-------------------------|-------------------------|-------------------------|-------------------------|
| | Acc. \uparrow | Forgetting \downarrow |
| Mamba-Seq | 63.72 \pm 0.55 | 28.52 \pm 0.49 | 56.95 \pm 0.62 | 36.37 \pm 0.53 | 49.01 \pm 0.35 | 53.94 \pm 0.39 | 39.36 \pm 0.58 | 64.74 \pm 0.63 |
| Mamba-CL | 81.67 \pm 0.37 | 4.07 \pm 0.33 | 78.60 \pm 0.41 | 4.88 \pm 0.39 | 89.60 \pm 0.27 | 2.57 \pm 0.36 | 85.03 \pm 0.48 | 3.52 \pm 0.54 |
| Upper-bound | 85.47 \pm 0.09 | - | 85.47 \pm 0.09 | - | 93.05 \pm 0.08 | - | 90.23 \pm 0.11 | - |

Table 2. Comparison with existing methods pre-trained on the ImageNet-21K. The results marked with \dagger and * are implemented by [7] and us, respectively, due to a lack of official results. The highest accuracies are in bold, and the second-highest accuracies are underlined.

| Method | Venue | 10-split ImageNet-R | | 20-split ImageNet-R | | 10-split CIFAR-100 | | 10-split DomainNet | |
|------------------|-----------|-------------------------|-------------------------|-------------------------|-------------------------|-------------------------|-------------------------|----------------------------|-------------------------|
| | | Acc. \uparrow | Forgetting \downarrow | Acc. \uparrow | Forgetting \downarrow | Acc. \uparrow | Forgetting \downarrow | Acc. \uparrow | Forgetting \downarrow |
| L2P [39] | CVPR'22 | 61.57 \pm 0.66 | 9.73 \pm 0.47 | 59.38 \pm 0.50 | 5.89 \pm 0.36 | 83.83 \pm 0.04 | 7.63 \pm 0.30 | 81.17 \pm 0.83 \dagger | 8.98 \pm 1.25 |
| DualPrompt [38] | ECCV'22 | 68.13 \pm 0.49 | 4.68 \pm 0.20 | 63.21 \pm 0.49 | 5.28 \pm 0.45 | 86.51 \pm 0.33 | 5.16 \pm 0.09 | 81.70 \pm 0.78 \dagger | 8.04 \pm 0.31 |
| CODA-Prompt [32] | CVPR'23 | 75.45 \pm 0.56 | 1.64 \pm 0.10 | 72.37 \pm 1.19 | 0.96 \pm 0.15 | 86.25 \pm 0.74 | 1.67 \pm 0.26 | 80.04 \pm 0.79 \dagger | 10.16 \pm 0.35 |
| LAE [6] | ICCV'23 | 72.66 \pm 0.63 | - | 69.67 \pm 0.86 | - | 85.59 \pm 0.46 | - | - | - |
| LGCL [16] | ICCV'23 | 69.46 \pm 0.04 | 4.20 \pm 0.06 | - | - | 87.23 \pm 0.21 | 5.10 \pm 0.15 | - | - |
| C-LN [3] | ICCVW'23 | 76.36 \pm 0.51 | 8.31 \pm 1.28 | 71.72 \pm 0.47 | 5.42 \pm 0.28 | 86.95 \pm 0.37 | 6.98 \pm 0.43 | - | - |
| ESN [37] | AAAI'23 | 71.07 \pm 0.29 | 4.99 \pm 0.49 | 64.77 \pm 0.71 | 6.65 \pm 1.24 | 86.34 \pm 0.52 | 4.76 \pm 0.14 | 79.22 \pm 2.04 \dagger | 10.62 \pm 2.12 |
| EvoPrompt [20] | AAAI'24 | 76.83 \pm 0.08 | 2.78 \pm 0.06 | 74.41 \pm 0.23 | 2.56 \pm 0.22 | 87.97 \pm 0.30 | 2.60 \pm 0.42 | 79.50 \pm 0.29* | 3.81 \pm 0.36 |
| PGP [28] | ICLR'24 | 69.34 \pm 0.05 | 4.53 \pm 0.04 | - | - | 86.92 \pm 0.05 | 5.35 \pm 0.19 | 80.41 \pm 0.25* | 8.39 \pm 0.18 |
| OVOR-Deep [13] | ICLR'24 | 76.11 \pm 0.21 | 7.16 \pm 0.34 | 73.85 \pm 0.29 | 6.80 \pm 0.65 | 85.99 \pm 0.89 | 6.42 \pm 2.03 | 79.61 \pm 0.86* | 4.77 \pm 0.94 |
| ConvPrompt [29] | CVPR'24 | <u>77.86</u> \pm 0.25 | 4.33 \pm 0.24 | <u>75.10</u> \pm 0.39 | 4.10 \pm 0.29 | <u>88.87</u> \pm 0.33 | 4.75 \pm 0.15 | 79.47 \pm 0.35* | 6.49 \pm 0.43 |
| InfLoRA [22] | CVPR'24 | 75.65 \pm 0.14 | 5.73 \pm 0.44 | 71.01 \pm 0.45 | 6.83 \pm 0.44 | 87.06 \pm 0.25 | 6.22 \pm 0.39 | 81.45 \pm 0.68* | 5.35 \pm 0.52 |
| EASE [44] | CVPR'24 | 76.17 | 7.82 | 73.27 | 8.51 | 87.76 | 5.94 | 78.89* | 7.89 |
| CPrompt [7] | CVPR'24 | 77.14 \pm 0.11 | 5.97 \pm 0.68 | 74.79 \pm 0.28 | 7.34 \pm 0.65 | 87.82 \pm 0.21 | 5.06 \pm 0.50 | <u>82.97</u> \pm 0.34 | 7.45 \pm 0.93 |
| Mamba-CL | This work | 81.67 \pm 0.37 | 4.07 \pm 0.33 | 78.60 \pm 0.41 | 4.88 \pm 0.39 | 89.60 \pm 0.27 | 2.57 \pm 0.36 | 85.03 \pm 0.48 | 3.52 \pm 0.54 |

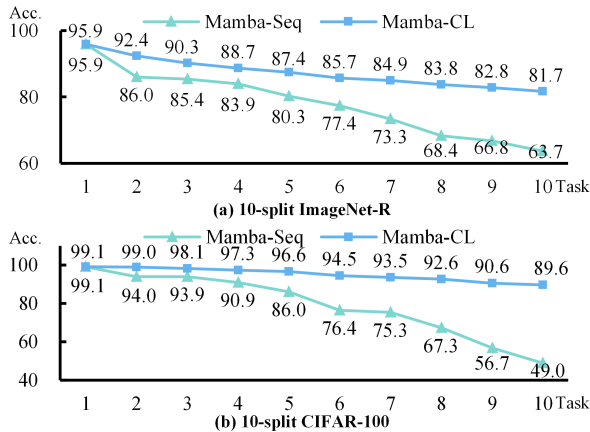


Figure 2. Task-by-task accuracy changing curves of the Mamba-Seq and the Mamba-CL on two benchmarks.

split ImageNet-R [11], 10-split CIFAR-100 [19] and 10-split DomainNet [27]. Note that the 10-split DomainNet is organized by Wang *et al.* [37] specifically for cross-domain CIL, with the top 200 classes from the original DomainNet [27] selected based on the number of samples. The

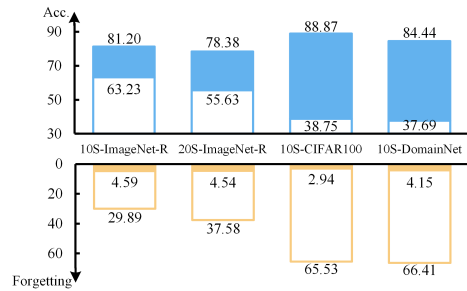


Figure 3. Results of using the pre-training parameters further fine-tuned on ImageNet-1k. The annotated values of the filled bars denote the accuracy or forgetting of Mamba-CL, while those of the blank bars denote the two metrics of the baseline.

above three datasets are also split into 50 or 100 tasks to evaluate the long-sequence continual learning performances.

Since only the De-focus Mamba-Large [34] has the weights pre-trained on ImageNet-21k [30] among existing visual Mamba models [10, 23, 45], we employ the De-focus Mamba-Large as the backbone, so that we can compare our approach with existing methods using the same pre-training dataset. More experimental results using the pre-

Table 3. Ablation study of the components proposed in our approach.

| $H_{1,\delta}$ | $H_{1,C}$ | H_2 | H_3 | H_{out} | 10S-ImageNet-R | | 20S-ImageNet-R | | 10S-CIFAR-100 | | 10S-DomainNet | |
|----------------|-----------|-------|-------|-----------|----------------|-------------|----------------|-------------|---------------|-------------|---------------|-------------|
| | | | | | Acc.↑ | Forgetting↓ | Acc.↑ | Forgetting↓ | Acc.↑ | Forgetting↓ | Acc.↑ | Forgetting↓ |
| | | | | | 63.72 | 28.52 | 56.95 | 36.37 | 49.01 | 53.94 | 39.36 | 64.74 |
| ✓ | | | | ✓ | 81.08 | 5.38 | 77.47 | 5.97 | 89.15 | 4.13 | 84.19 | 7.09 |
| | ✓ | | | ✓ | 79.92 | 7.30 | 76.45 | 8.53 | 87.90 | 6.94 | 83.02 | 8.91 |
| | | ✓ | | ✓ | 79.55 | 7.95 | 75.95 | 9.05 | 87.58 | 7.44 | 82.66 | 10.14 |
| | | | ✓ | ✓ | 79.75 | 7.82 | 76.38 | 8.76 | 88.12 | 6.76 | 83.05 | 9.20 |
| ✓ | ✓ | ✓ | ✓ | | 79.42 | 8.25 | 76.23 | 8.91 | 87.79 | 6.98 | 82.89 | 9.31 |
| | | | | ✓ | 78.25 | 9.14 | 75.53 | 9.73 | 87.28 | 7.67 | 81.98 | 11.26 |
| ✓ | ✓ | ✓ | ✓ | ✓ | 81.67 | 4.07 | 78.60 | 4.88 | 89.60 | 2.57 | 85.03 | 3.52 |

Table 4. Results for long-sequence continual learning under the settings of 50 tasks and 100 tasks across five benchmarks.

| Method | Venue | 50S-ImageNet-R | | 50S-CIFAR-100 | | 50S-DomainNet | | 100S-ImageNet-R | | 100S-DomainNet | |
|----------------|-----------|----------------|------------|---------------|------------|---------------|------------|-----------------|------------|----------------|------------|
| | | Acc. | Forgetting | Acc. | Forgetting | Acc. | Forgetting | Acc. | Forgetting | Acc. | Forgetting |
| L2P [39] | CVPR'22 | 48.53 | 12.99 | 76.19 | 12.06 | 59.45 | 11.53 | 38.87 | 15.26 | 50.52 | 17.66 |
| EvoPrompt [20] | AAAI'24 | <u>68.53</u> | 10.03 | <u>76.60</u> | 13.86 | 67.68 | 10.41 | <u>61.84</u> | 15.84 | <u>56.35</u> | 21.39 |
| OVOR-Deep [13] | ICLR'24 | 60.08 | 5.86 | 65.69 | 14.28 | 66.27 | 7.43 | 40.49 | 8.12 | 47.65 | 8.91 |
| InfLoRA [22] | CVPR'24 | 59.02 | 11.02 | 61.49 | 13.68 | <u>69.96</u> | 9.51 | 38.16 | 15.11 | 44.32 | 17.85 |
| EASE [44] | CVPR'24 | 68.17 | 7.76 | 74.47 | 9.31 | 61.20 | 10.01 | 47.55 | 8.22 | 33.08 | 32.14 |
| CPrompt [7] | CVPR'24 | 68.47 | 8.16 | 74.97 | 7.45 | 67.87 | 9.36 | 56.95 | 10.20 | 53.73 | 12.14 |
| Mamba-Seq | Baseline | 19.77 | 72.81 | 11.13 | 85.63 | 4.05 | 94.89 | 7.33 | 79.93 | 2.57 | 81.98 |
| Mamba-CL | This work | 70.47 | 4.91 | 81.05 | 6.01 | 72.33 | 11.69 | 63.05 | 8.76 | 57.91 | 14.12 |

training weights of ImageNet-1k are provided in Appendix C.2. The null-space projection matrix for the liner layer after the SSM is computed in the same way as that in linear/convolutional layers [36]. We use the Adam [17] optimizer to train the backbone for 50 epochs with an initial learning rate of 0.0002 and a batch size of 200. The learning rate of the classifier is set to 0.01. We report the mean values of the final average accuracy and final average forgetting over three runs with different random seeds. Additional experimental details can be found in the Appendix.

5.2. Validation of Effectiveness

Comparison with Baseline: We conduct experiments on four benchmarks involving two regular-sequence settings (*i.e.*, 10 and 20 tasks). The results are presented in Table 1. The baseline employing sequential fine-tuning without null-space projections is represented by "-Seq". Our approach using the proposed null-space projections is denoted by "-CL". The proposed Mamba-CL outperforms the baseline by a large margin, enhancing accuracy by 18%~45% and reducing forgetting by 24%~61% across all benchmarks.

Figure 2 visually depicts the accuracy curves for the 10-split ImageNet-R and CIFAR-100. The performance of the Mamba-CL surpasses the baseline on each task consistently. Especially, the improvement increases with learning more

and more tasks. Furthermore, we also validate that our approach performs well on different pre-training parameters. As shown in Figure 3, when using the pre-training parameters pre-trained on ImageNet-21k and further fine-tuned on ImageNet-1k, the Mamba-CL can still bring significant accuracy improvements.

Evolution of Training Loss: To validate the stability of the proposed Mamba-CL on old tasks, we visualize the evolution of training losses on tasks \mathcal{T}_1 and \mathcal{T}_2 across two benchmarks, as shown in Figure 5. Each data point on the curves represents the loss value of the training data in $\mathcal{T}_1/\mathcal{T}_2$ after continuously training Mamba on a new task. It can be observed that when Mamba is trained with the proposed null-space method, the training losses for these two old tasks remain almost unchanged. This indicates that the representations of previous instances do not change during training new tasks, thus enabling the model to learn new tasks without compromising performance on previously learned tasks.

Comparison with Existing Approaches: We compare the proposed method with existing state-of-the-art methods across four benchmarks, as shown in Table 2. Our method Mamba-CL demonstrates an average improvement of 2.5% and a maximum improvement of 3.8% in accuracy over other leading methods across these four benchmarks, showcasing the superiority of the proposed approach. Although

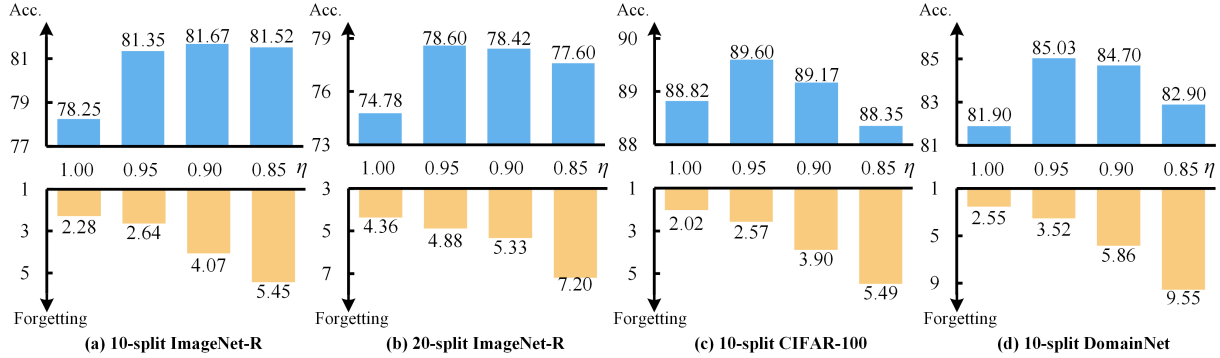


Figure 4. Effects of the orthogonal projection weight η on accuracy and forgetting for the stability-plasticity trade-off.

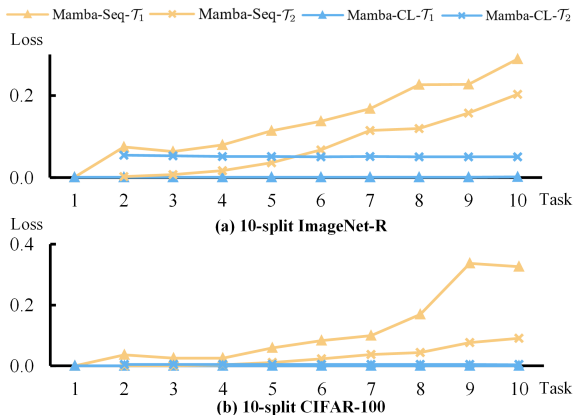


Figure 5. The change of training losses on tasks \mathcal{T}_1 and \mathcal{T}_2 of the baseline Mamba-Seq and our approach Mamba-CL.

Mamba-CL does not achieve the lowest forgetting, this is attributed to the dual influence of stability and plasticity on accuracy. By allowing a slight increase in forgetting, we can strike a balance in the stability-plasticity trade-off, thereby enhancing the model’s overall accuracy.

5.3. Further Analysis

Ablation Study: Our approach comprises three key components, *i.e.*, the three null-space projection matrices $\mathbf{H}_{\{1,2,3\}}$. We use $\mathbf{H}_{1,\delta}$ and $\mathbf{H}_{1,C}$ to differentiate the \mathbf{H}_1 performed on δ and C , respectively. As aforementioned, the linear layer after SSM is also trained with a null-space projection matrix, which is denoted as \mathbf{H}_{out} . The effect of the introduced projection matrices is shown in Table 3. We can conclude that: 1) among the four projections for the SSM, the projection of δ (*i.e.*, $\mathbf{H}_{1,\delta}$) plays the most important role in anti-forgetting. This is reasonable since the parameters \mathbf{A} and \mathbf{B} are both discretized by δ . 2) The null-space projection applied to the input-invariant parameter \mathbf{A} (*i.e.*, \mathbf{H}_2) has a relatively minor impact. 3) When the projection matrices are employed jointly, the model achieves the best accuracy with the least forgetting. This demonstrates that the proposed null-space projections can collectively contribute to Mamba’s stability in continual learning.

Long-sequence Continual Learning: To verify that our

approach is also suitable for long-sequence continual learning, we conduct experiments across five CIL benchmarks, with task counts reaching 50 and 100, as shown in Table 4. We additionally reproduce six existing leading methods for comparison. The results indicate that the baseline Mamba-Seq without anti-forgetting mechanism performs poorly in long-sequence continual learning tasks. In contrast, Mamba-CL achieves a substantial improvement in accuracy over Mamba-Seq and a significant reduction in forgetting. Compared with other outstanding methods, Mamba-CL outperforms the second-best approach by an average of 2.3%, with a maximum improvement of 4.5%. This demonstrates that the proposed null-space projection method enables Mamba-CL to maintain its advantage in long-sequence continual learning.

Trade-off between Stability and Plasticity: As described in Section 4.2, we introduce a hyper-parameter $\eta \in [0, 1]$ for the null-space projection matrix to balance stability and plasticity. Figure 4 displays the effects of η on accuracy and forgetting. Although the forgetting is lowest when η is set to 1, the accuracy is limited due to the weakened model plasticity. As η decreases from 1 to 0.85 in steps of 0.05, the accuracy initially increases before decreasing, while the forgetting consistently rises. This trend indicates a gradual reduction in model stability and an increase in plasticity. When an optimal balance between stability and plasticity is reached (*i.e.*, $\eta=0.90$ for 10-split ImageNet-R and 0.95 for other benchmarks), the model reaches peak accuracy.

6. Conclusion

In this paper, we introduce Mamba-CL, the first method to incorporate orthogonal projection into the Mamba model for continual learning. This approach enables continuous training of the large-scale Mamba foundation model without catastrophic forgetting, ensuring the output from each SSM block remain consistent across both previous and current tasks. We derive four sufficient orthogonal conditions on the key time-invariant parameters in the SSM block to optimize the Mamba model for continual learning, and apply a null-space-based approximation to

efficiently implement these gradient projection conditions. In future work, we aim to explore more flexible constraints on orthogonal projections and extend our method to more variants of Mamba foundation models.

References

- [1] Rahaf Aljundi, Min Lin, Baptiste Goujaud, and Yoshua Bengio. Gradient based sample selection for online continual learning. *Advances in neural information processing systems*, 32, 2019. 1
- [2] Ekin D Cubuk, Barret Zoph, Dandelion Mane, Vijay Vasudevan, and Quoc V Le. Autoaugment: Learning augmentation strategies from data. In *Proceedings of the IEEE/CVF conference on computer vision and pattern recognition*, pages 113–123, 2019. 13
- [3] Thomas De Min, Massimiliano Mancini, Karteek Alahari, Xavier Alameda-Pineda, and Elisa Ricci. On the effectiveness of layernorm tuning for continual learning in vision transformers. In *2023 IEEE/CVF International Conference on Computer Vision Workshops (ICCVW)*, pages 3577–3586. IEEE, 2023. 6
- [4] Danruo Deng, Guangyong Chen, Jianye Hao, Qiong Wang, and Pheng-Ann Heng. Flattening sharpness for dynamic gradient projection memory benefits continual learning. *Advances in Neural Information Processing Systems*, 34: 18710–18721, 2021. 2
- [5] Qiang Gao, Zhipeng Luo, Diego Klabjan, and Fengli Zhang. Efficient architecture search for continual learning. *IEEE Transactions on Neural Networks and Learning Systems*, 34 (11):8555–8565, 2022. 1
- [6] Qiankun Gao, Chen Zhao, Yifan Sun, Teng Xi, Gang Zhang, Bernard Ghanem, and Jian Zhang. A unified continual learning framework with general parameter-efficient tuning. In *Proceedings of the IEEE/CVF International Conference on Computer Vision*, pages 11483–11493, 2023. 6
- [7] Zhanxin Gao, Jun Cen, and Xiaobin Chang. Consistent prompting for rehearsal-free continual learning. In *Proceedings of the IEEE/CVF Conference on Computer Vision and Pattern Recognition*, pages 28463–28473, 2024. 2, 6, 7, 11, 12, 13
- [8] Albert Gu and Tri Dao. Mamba: Linear-time sequence modeling with selective state spaces. *arXiv preprint arXiv:2312.00752*, 2023. 1, 2, 3
- [9] Albert Gu, Karan Goel, and Christopher Ré. Efficiently modeling long sequences with structured state spaces. *arXiv preprint arXiv:2111.00396*, 2021. 1, 2
- [10] Ali Hatamizadeh and Jan Kautz. Mambavision: A hybrid mamba-transformer vision backbone. *arXiv preprint arXiv:2407.08083*, 2024. 6, 11, 12, 13
- [11] Dan Hendrycks, Steven Basart, Norman Mu, Saurav Kadavath, Frank Wang, Evan Dorundo, Rahul Desai, Tyler Zhu, Samyak Parajuli, Mike Guo, et al. The many faces of robustness: A critical analysis of out-of-distribution generalization. In *Proceedings of the IEEE/CVF international conference on computer vision*, pages 8340–8349, 2021. 6
- [12] Qinghua Hu, Yucong Gao, and Bing Cao. Curiosity-driven class-incremental learning via adaptive sample selection. *IEEE Transactions on Circuits and Systems for Video Technology*, 32(12):8660–8673, 2022. 1
- [13] Wei-Cheng Huang, Chun-Fu Chen, and Hsiang Hsu. OVOR: Oneprompt with virtual outlier regularization for rehearsal-free class-incremental learning. In *The Twelfth International Conference on Learning Representations*, 2024. 6, 7
- [14] Ching-Yi Hung, Cheng-Hao Tu, Cheng-En Wu, Chien-Hung Chen, Yi-Ming Chan, and Chu-Song Chen. Compacting, picking and growing for unforgetting continual learning. *Advances in neural information processing systems*, 32, 2019. 1
- [15] Md Mohaiminul Islam, Mahmudul Hasan, Kishan Shamsundar Athrey, Tony Braskich, and Gedas Bertasius. Efficient movie scene detection using state-space transformers. In *Proceedings of the IEEE/CVF Conference on Computer Vision and Pattern Recognition*, pages 18749–18758, 2023. 2
- [16] Muhammad Gul Zain Ali Khan, Muhammad Ferjad Naeem, Luc Van Gool, Didier Stricker, Federico Tombari, and Muhammad Zeshan Afzal. Introducing language guidance in prompt-based continual learning. In *Proceedings of the IEEE/CVF International Conference on Computer Vision*, pages 11463–11473, 2023. 6
- [17] Diederik P Kingma. Adam: A method for stochastic optimization. *arXiv preprint arXiv:1412.6980*, 2014. 7, 13
- [18] James Kirkpatrick, Razvan Pascanu, Neil Rabinowitz, Joel Veness, Guillaume Desjardins, Andrei A Rusu, Kieran Milan, John Quan, Tiago Ramalho, Agnieszka Grabska-Barwinska, et al. Overcoming catastrophic forgetting in neural networks. *Proceedings of the national academy of sciences*, 114(13):3521–3526, 2017. 1, 2
- [19] Alex Krizhevsky, Geoffrey Hinton, et al. Learning multiple layers of features from tiny images. 2009. 6, 11
- [20] Muhammad Rifki Kurniawan, Xiang Song, Zhiheng Ma, Yuhang He, Yihong Gong, Yang Qi, and Xing Wei. Evolving parameterized prompt memory for continual learning. In *Proceedings of the AAAI Conference on Artificial Intelligence*, pages 13301–13309, 2024. 6, 7
- [21] Yan-Shuo Liang and Wu-Jun Li. Adaptive plasticity improvement for continual learning. In *Proceedings of the IEEE/CVF Conference on Computer Vision and Pattern Recognition*, pages 7816–7825, 2023. 2, 4
- [22] Yan-Shuo Liang and Wu-Jun Li. Inflora: Interference-free low-rank adaptation for continual learning. In *Proceedings of the IEEE/CVF Conference on Computer Vision and Pattern Recognition*, pages 23638–23647, 2024. 6, 7, 12, 13
- [23] Yue Liu, Yunjie Tian, Yuzhong Zhao, Hongtian Yu, Lingxi Xie, Yaowei Wang, Qixiang Ye, and Yunfan Liu. Vmamba: Visual state space model. *arXiv preprint arXiv:2401.10166*, 2024. 2, 6, 11, 12, 13
- [24] Yue Lu, Shizhou Zhang, De Cheng, Yinghui Xing, Nannan Wang, Peng Wang, and Yanning Zhang. Visual prompt tuning in null space for continual learning. *Advances in neural information processing systems*, 2024. 1, 2, 3, 5
- [25] Jun Ma, Feifei Li, and Bo Wang. U-mamba: Enhancing long-range dependency for biomedical image segmentation. *arXiv preprint arXiv:2401.04722*, 2024. 2

- [26] Adam Paszke, Sam Gross, Francisco Massa, Adam Lerer, James Bradbury, Gregory Chanan, Trevor Killeen, Zeming Lin, Natalia Gimelshein, Luca Antiga, et al. Pytorch: An imperative style, high-performance deep learning library. *Advances in neural information processing systems*, 32, 2019. 13
- [27] Xingchao Peng, Qinxun Bai, Xide Xia, Zijun Huang, Kate Saenko, and Bo Wang. Moment matching for multi-source domain adaptation. In *Proceedings of the IEEE/CVF international conference on computer vision*, pages 1406–1415, 2019. 6, 11
- [28] Jingyang Qiao, Xin Tan, Chengwei Chen, Yanyun Qu, Yong Peng, Yuan Xie, et al. Prompt gradient projection for continual learning. In *The Twelfth International Conference on Learning Representations*, 2023. 2, 6
- [29] Anurag Roy, Riddhiman Moulick, Vinay K Verma, Saptarshi Ghosh, and Abir Das. Convolutional prompting meets language models for continual learning. In *Proceedings of the IEEE/CVF Conference on Computer Vision and Pattern Recognition*, pages 23616–23626, 2024. 6
- [30] Olga Russakovsky, Jia Deng, Hao Su, Jonathan Krause, Sanjeev Satheesh, Sean Ma, Zhiheng Huang, Andrej Karpathy, Aditya Khosla, Michael Bernstein, et al. Imagenet large scale visual recognition challenge. *International journal of computer vision*, 115:211–252, 2015. 6, 11
- [31] Gobinda Saha, Isha Garg, and Kaushik Roy. Gradient projection memory for continual learning. *arXiv preprint arXiv:2103.09762*, 2021. 2, 4, 5
- [32] James Seale Smith, Leonid Karlinsky, Vyshnavi Gutta, Paola Cascante-Bonilla, Donghyun Kim, Assaf Arbelle, Rameswar Panda, Rogerio Feris, and Zsolt Kira. Coda-prompt: Continual decomposed attention-based prompting for rehearsal-free continual learning. In *Proceedings of the IEEE/CVF Conference on Computer Vision and Pattern Recognition*, pages 11909–11919, 2023. 2, 6, 12, 13
- [33] Jimmy TH Smith, Andrew Warrington, and Scott W Linderman. Simplified state space layers for sequence modeling. *arXiv preprint arXiv:2208.04933*, 2022. 1, 2
- [34] Chenxin Tao, Xizhou Zhu, Shiqian Su, Lewei Lu, Changyao Tian, Xuan Luo, Gao Huang, Hongsheng Li, Yu Qiao, Jie Zhou, et al. Learning 1d causal visual representation with defocus attention networks. *arXiv preprint arXiv:2406.04342*, 2024. 1, 2, 3, 6, 11
- [35] Jue Wang, Wentao Zhu, Pichao Wang, Xiang Yu, Linda Liu, Mohamed Omar, and Raffay Hamid. Selective structured state-spaces for long-form video understanding. In *Proceedings of the IEEE/CVF Conference on Computer Vision and Pattern Recognition*, pages 6387–6397, 2023. 2
- [36] Shipeng Wang, Xiaorong Li, Jian Sun, and Zongben Xu. Training networks in null space of feature covariance for continual learning. In *Proceedings of the IEEE/CVF conference on Computer Vision and Pattern Recognition*, pages 184–193, 2021. 1, 2, 4, 5, 7, 11
- [37] Yabin Wang, Zhiheng Ma, Zhiwu Huang, Yaowei Wang, Zhou Su, and Xiaopeng Hong. Isolation and impartial aggregation: A paradigm of incremental learning without interference. In *Proceedings of the AAAI Conference on Artificial Intelligence*, pages 10209–10217, 2023. 6, 11
- [38] Zifeng Wang, Zizhao Zhang, Sayna Ebrahimi, Ruoxi Sun, Han Zhang, Chen-Yu Lee, Xiaoqi Ren, Guolong Su, Vincent Perot, Jennifer Dy, et al. Dualprompt: Complementary prompting for rehearsal-free continual learning. In *European Conference on Computer Vision*, pages 631–648. Springer, 2022. 2, 3, 6, 11
- [39] Zifeng Wang, Zizhao Zhang, Chen-Yu Lee, Han Zhang, Ruoxi Sun, Xiaoqi Ren, Guolong Su, Vincent Perot, Jennifer Dy, and Tomas Pfister. Learning to prompt for continual learning. In *Proceedings of the IEEE/CVF conference on computer vision and pattern recognition*, pages 139–149, 2022. 2, 3, 6, 7, 12
- [40] Ross Wightman. Pytorch image models. <https://github.com/rwightman/pytorch-image-models>, 2019. 13
- [41] Jaehong Yoon, Saehoon Kim, Eunho Yang, and Sung Ju Hwang. Scalable and order-robust continual learning with additive parameter decomposition. *International Conference on Learning Representations*, 2020. 1
- [42] Guanxiong Zeng, Yang Chen, Bo Cui, and Shan Yu. Continual learning of context-dependent processing in neural networks. *Nature Machine Intelligence*, 1(8):364–372, 2019. 1, 2
- [43] Hanbin Zhao, Hui Wang, Yongjian Fu, Fei Wu, and Xi Li. Memory-efficient class-incremental learning for image classification. *IEEE Transactions on Neural Networks and Learning Systems*, 33(10):5966–5977, 2021. 1
- [44] Da-Wei Zhou, Hai-Long Sun, Han-Jia Ye, and De-Chuan Zhan. Expandable subspace ensemble for pre-trained model-based class-incremental learning. In *Proceedings of the IEEE/CVF Conference on Computer Vision and Pattern Recognition*, pages 23554–23564, 2024. 6, 7
- [45] Lianghui Zhu, Bencheng Liao, Qian Zhang, Xinlong Wang, Wenyu Liu, and Xinggang Wang. Vision mamba: Efficient visual representation learning with bidirectional state space model. *arXiv preprint arXiv:2401.09417*, 2024. 1, 2, 6, 11, 12, 13

Mamba-CL: Optimizing Selective State Space Model in Null Space for Continual Learning

Supplementary Material

A. The Whole Training Process

The whole training process is outlined in Algorithm 1.

Algorithm 1 Null Space Optimization for Mamba-CL.

Inputs: Datasets $\mathcal{D}_t = \{(\mathcal{X}_t^{<i>}, y_t^{<i>})\}_{i=1}^{|\mathcal{T}_t|}$ for task $\mathcal{T}_t \in \{\mathcal{T}_1, \mathcal{T}_2, \dots\}$, the Mamba model $f(\cdot)$ with learnable parameters $\{\mathbf{A}_{t-1}, \mathbf{W}_{t-1}^B, \mathbf{W}_{t-1}^C, \mathbf{W}_{t-1}^\delta\}$, the uncentered covariance matrices $\{\mathbf{Q}_1, \mathbf{Q}_2, \mathbf{Q}_3\}$, the projection matrices $\{\mathbf{H}_1, \mathbf{H}_2, \mathbf{H}_3\}$, learning rate γ .

Outputs: Optimized parameters $\{\mathbf{A}_t, \mathbf{W}_t^B, \mathbf{W}_t^C, \mathbf{W}_t^\delta\}$.

- 1: **Initialization:** Randomly initialize parameters $\{\mathbf{A}_0, \mathbf{W}_0^B, \mathbf{W}_0^C, \mathbf{W}_0^\delta\}; \{\mathbf{Q}_1, \mathbf{Q}_2, \mathbf{Q}_3\} = \{\mathbf{0}, \mathbf{0}, \mathbf{0}\};$
 - 2: **for** task $\mathcal{T}_t \in \{\mathcal{T}_1, \mathcal{T}_2, \dots\}$ **do**
 - 3: **repeat**
 - 4: Sample a mini-batch $\mathcal{X}_t, y_t \sim \mathcal{D}_t;$
 - 5: Get $\hat{y}_t \leftarrow f(\mathcal{X}_t | \mathbf{A}_{t-1}, \mathbf{W}_{t-1}^B, \mathbf{W}_{t-1}^C, \mathbf{W}_{t-1}^\delta);$
 - 6: Compute loss $\mathcal{L} \leftarrow \text{CrossEntropy}(\hat{y}_t, y_t);$
 - 7: Backward propagation;
 - 8: Get the gradients $\mathbf{G}^A, \mathbf{G}^B, \mathbf{G}^C, \mathbf{G}^\delta;$
 - 9: **if** $t > 1$ **then**
 - 10: Update \mathbf{W}^δ by $\mathbf{W}_{t-1}^\delta \leftarrow \mathbf{W}_{t-1}^\delta - \gamma \mathbf{H}_1 \mathbf{G}^\delta;$
 - 11: Update \mathbf{W}^C by $\mathbf{W}_{t-1}^C \leftarrow \mathbf{W}_{t-1}^C - \gamma \mathbf{H}_1 \mathbf{G}^C;$
 - 12: Update \mathbf{A} by $\mathbf{A}_{t-1} \leftarrow \mathbf{A}_{t-1} - \gamma \mathbf{H}_2 \mathbf{G}^A;$
 - 13: Update \mathbf{W}^B by $\mathbf{W}_{t-1}^B \leftarrow \mathbf{W}_{t-1}^B - \gamma \mathbf{H}_3 \mathbf{G}^B;$
 - 14: **else**
 - 15: Update \mathbf{W}^δ by $\mathbf{W}_{t-1}^\delta \leftarrow \mathbf{W}_{t-1}^\delta - \gamma \mathbf{G}^\delta;$
 - 16: Update \mathbf{W}^C by $\mathbf{W}_{t-1}^C \leftarrow \mathbf{W}_{t-1}^C - \gamma \mathbf{G}^C;$
 - 17: Update \mathbf{A} by $\mathbf{A}_{t-1} \leftarrow \mathbf{A}_{t-1} - \gamma \mathbf{G}^A;$
 - 18: Update \mathbf{W}^B by $\mathbf{W}_{t-1}^B \leftarrow \mathbf{W}_{t-1}^B - \gamma \mathbf{G}^B;$
 - 19: **end if**
 - 20: **until** convergence
 - 21: Get optimized parameters $\{\mathbf{A}_t, \mathbf{W}_t^B, \mathbf{W}_t^C, \mathbf{W}_t^\delta\} = \{\mathbf{A}_{t-1}, \mathbf{W}_{t-1}^B, \mathbf{W}_{t-1}^C, \mathbf{W}_{t-1}^\delta\};$
 - 22: Initialize three temporary matrices $\mathbf{J}_1 = [], \mathbf{J}_2 = []$ and $\mathbf{J}_3 = [];$
 - 23: **for** $\mathcal{X}_t^{<i>} \in \mathcal{D}_t$ **do**
 - 24: Get the feature matrices $(\mathbf{X}_t)^{<i>}, (\delta_t)^{<i>}$ and $(\delta_t \mathbf{X}_t)^{<i>}$ through the forward propagation;
 - 25: Update $\mathbf{J}_1, \mathbf{J}_2$ and \mathbf{J}_3 by concatenating $(\mathbf{X}_t)^{<i>}, (\delta_t)^{<i>}$ and $(\delta_t \mathbf{X}_t)^{<i>},$ respectively;
 - 26: **end for**
 - 27: Update uncentered covariance matrices $\mathbf{Q}_1 \leftarrow \mathbf{Q}_1 + \mathbf{J}_1^\top \mathbf{J}_1, \mathbf{Q}_2 \leftarrow \mathbf{Q}_2 + \mathbf{J}_2^\top \mathbf{J}_2$ and $\mathbf{Q}_3 \leftarrow \mathbf{Q}_3 + \mathbf{J}_3^\top \mathbf{J}_3;$
 - 28: Compute the projection matrices $\{\mathbf{H}_1, \mathbf{H}_2, \mathbf{H}_3\}$ by SVD on $\{\mathbf{Q}_1, \mathbf{Q}_2, \mathbf{Q}_3\}.$
 - 29: **end for**
-

B. Experimental Setups and Implementation Details

B.1. Models

As we investigated, only the De-focus Mamba-Large [34] provides the pre-training weights on the ImageNet-21k dataset [30], while other variants such as De-focus Mamba-Base [34], MambaVision [10], VMamba [23] and Vim [45] only have the pre-training weights on the ImageNet-1k dataset. To compare with existing ViT-based methods which are pre-trained on ImageNet-21k, we mainly employ the De-focus Mamba-Large which is also pre-trained on ImageNet-21k as the backbone in our experiments. In order to further verify the generalizability of our approach across various Mamba variants and compare with existing ViT-based models under similar backbones as well as the same pre-training weights, we also experiment on MambaVision [10], Vim [45] and VMamba [23] which are pre-trained on the ImageNet-1k dataset, whose results are shown in Section C.2.

There are 48 Mamba blocks in the backbone and the SSM in every Mamba block is fine-tuned with the proposed null-space projection. In addition, the linear layer after the SSM within the Mamba block is also fine-tuned with the null-space projection derived from linear layers [36]. We conduct an ablation study in Section C.1 to determine which linear layer within the Mamba block to fine-tune by observing the adaptation performance on downstream tasks. The classifiers are trained for each task independently. During inference, all classifiers from previous tasks are concatenated to make predictions for all available classes.

B.2. Benchmarks

We conduct experiments under the class-incremental learning protocol, where the classes in each task are disjoint, and task identity is unknown during inference. Four class-incremental benchmarks across three widely used datasets are adopted: 10-split and 20-split ImageNet-R [38], 10-split CIFAR-100 [19] and 10-split DomainNet [27, 37].

We follow [38] to randomly split the 200 classes in ImageNet-R into 10 and 20 tasks, forming the 10-split and 20-split ImageNet-R benchmarks, respectively, aiming to evaluate the ability to handle different numbers of tasks. For the CIFAR-100 dataset, the total 100 classes are randomly split into 10 tasks. Note that the DomainNet [27] was originally proposed for domain-incremental learning. However, we follow the same dataset protocol adopted in [37] and [7]

Table 5. Results of using three different backbones pre-trained on the ImageNet-1k dataset.

| Backbone | Method | 10S-ImageNet-R | | 20S-ImageNet-R | | 10S-CIFAR-100 | | 10S-DomainNet | |
|------------------|------------------|----------------|------------|----------------|------------|---------------|------------|---------------|------------|
| | | Acc. | Forgetting | Acc. | Forgetting | Acc. | Forgetting | Acc. | Forgetting |
| MambaVision [10] | Mamba-Seq | 64.38 | 25.02 | 64.17 | 26.55 | 65.72 | 33.89 | 62.01 | 37.94 |
| | Mamba-CL | 76.18 | 7.81 | 73.58 | 8.74 | 77.41 | 15.30 | 76.14 | 17.21 |
| Vim [45] | Mamba-Seq | 65.21 | 23.54 | 64.19 | 24.96 | 67.24 | 29.31 | 61.23 | 38.44 |
| | Mamba-CL | 75.39 | 8.16 | 73.27 | 8.79 | 78.43 | 14.34 | 75.68 | 18.12 |
| VMamba [23] | Mamba-Seq | 64.05 | 25.92 | 63.52 | 26.10 | 65.98 | 30.76 | 62.06 | 37.25 |
| | Mamba-CL | 75.89 | 7.95 | 72.96 | 9.39 | 76.87 | 15.81 | 77.11 | 16.64 |
| ViT | CODA-Prompt [32] | 67.68 | 4.81 | 64.56 | 5.78 | 75.79 | 4.17 | 63.61 | 6.19 |
| | CPrompt [7] | 59.27 | 5.98 | 53.07 | 4.49 | 71.97 | 7.91 | 69.34 | 5.78 |
| | InfLoRA [22] | 69.47 | 5.63 | 67.42 | 5.93 | 76.56 | 8.68 | 76.82 | 6.34 |

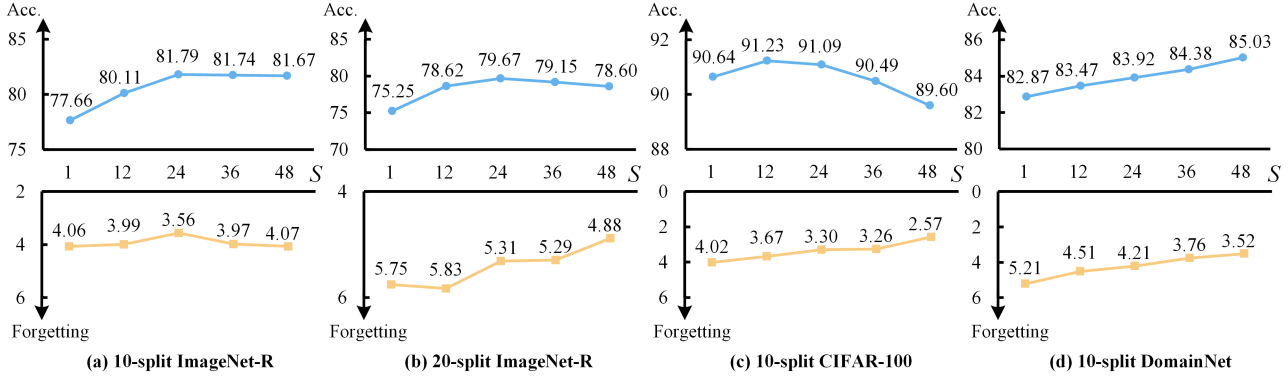


Figure 6. Performance with regard to the number of fine-tuned Mamba blocks (S). The first $\{1, 12, 14, 36, 48\}$ Mamba blocks are fine-tuned and the rest blocks are kept frozen.

Table 6. Joint training accuracy (%) of training different additional layers in the Mamba block. 'None' means only fine-tuning the SSM without training additional layers.

| Layer | ImageNet-R | CIFAR-100 | DomainNet |
|-----------------------|--------------|--------------|--------------|
| None | 84.03 | 92.13 | 89.37 |
| Linear _{in1} | 85.32 | 92.64 | 90.06 |
| Linear _{in2} | 84.68 | 92.51 | 89.47 |
| Causal Conv | 85.12 | 92.78 | 89.68 |
| Linear _{out} | 85.47 | 93.05 | 90.23 |

to select the top 200 classes with the most images from the original DomainNet, and randomly split them into 10 tasks with 20 classes per task to construct a cross-domain class-incremental benchmark.

B.3. Metrics

Following [39] and most continual learning methods based on pre-training, we report the final average accuracy and

the final average forgetting in our paper. Formally, the final average accuracy and final average forgetting are defined as:

$$\text{Accuracy} = \frac{1}{T} \sum_{i=1}^T a_{T,i},$$

$$\text{Forgetting} = \frac{1}{T-1} \sum_{i=1}^{T-1} \max_{j \in \{1, 2, \dots, T-1\}} (a_{j,i} - a_{T,i}),$$

where T is the number of tasks, $a_{T,i}$ is the accuracy of the T -th model on the i -th task data, and $a_{j,i}$ is the accuracy of the j -th model on the i -th task samples.

Note that the aforementioned final average accuracy is the commonly used metric in pre-training-based works. However, in addition to the final average accuracy, a few works also report mean average accuracy, which is defined as the mean value of the final average accuracies for all tasks. For a fair comparison, we consistently report the final average accuracy for all the methods in our paper.

Higher accuracy indicates better model performance,

while lower forgetting signifies stronger stability (*i.e.*, the ability to retain old knowledge). However, lower forgetting does not always lead to higher accuracy, as accuracy is also influenced by plasticity (*i.e.*, the ability to learn new knowledge). Accuracy is the primary metric that we should focus on, as it reflects the precision of classification in practice.

B.4. Implementation Details

The images fed into the models are resized to 192×192 pixels and augmented by AutoAugment [2] during training. We use the Adam optimizer [17] with $\beta_1 = 0.9$, $\beta_2 = 0.999$ and a weight decay of 5×10^{-5} to train the backbone for 50 epochs with an initial learning rate of 0.0002 and a batch size of 200. The learning rate is scaled by a factor of 0.1 at the 25-th and 40-th epochs. For the classifier, we use a large learning rate of 0.01 to promote the adaptation to downstream tasks. Our training loss only involves the cross-entropy loss for classification.

As introduced in the Optimization of Consistency Conditions section, we adopt a balanced hyper-parameter η for the trade-off between stability and plasticity in the null-space projections. η is set to 0.90 for 10-split ImageNet-R and 0.95 for other benchmarks.

We implement our approach in PyTorch [26] with the timm library [40]. The experiments are performed on a server with 128 GB RAM and four NVIDIA RTX 4090 GPUs.

C. More Experimental Results

C.1. Determination of Additional Linear Layer

To promote the model’s adaptation to downstream tasks, we additionally train an extra layer within the Mamba block alongside the SSM. We denote the linear layers before the SSM in the left and right branches as Linear_1 and Linear_2 , respectively, and the linear layer after the SSM as $\text{Linear}_{\text{out}}$. In addition, there is a Causal Conv layer preceding the SSM. The layer to be additionally trained is determined based on the joint training accuracy of the model on the datasets. As shown in Table 6, the model exhibits the best adaptation ability in downstream tasks when the $\text{Linear}_{\text{out}}$ is additionally fine-tuned. Therefore, in our experiments, we fine-tune both the SSM and the $\text{Linear}_{\text{out}}$ layer.

C.2. Generalizability across Visual Mamba Variants

To validate that our proposed Mamba-CL is applicable to other visual mamba variants, we conduct experiments on the four benchmarks using the MambaVision [10], Vim [45] and VMamba [23] backbones of their corresponding *base versions*. Moreover, we use the official codes to reproduce three ViT-based methods whose backbones are ViT-B/16: CODA-Prompt [32] (CVPR’23), CPrompt [7] (CVPR’24)

and InfLoRA [22] (CVPR’24). All of these Mamba-based and ViT-based models are *pre-trained on the ImageNet-1k dataset*. The results are shown in Table 5. It can be seen that our approach improves accuracy by 9%~14% across the three backbones on the benchmarks, and reduces forgetting by 15%~20%. The proposed Mamba-CL exhibits good generalizability in multiple variants of visual Mambas. Moreover, the Mamba-CL method can outperform the other three ViT-based methods, demonstrating the superiority of the proposed approach.

C.3. Number of Fine-tuned Mamba Blocks

There are 48 Mamba blocks in the De-focus Mamba-Large model. We fine-tune the first {1, 12, 24, 36, 48} blocks and freeze the rest blocks. The accuracy and forgetting are shown in Figure 6.

The accuracy first increases significantly and then decreases slightly on ImageNet-R and CIFAR-100 datasets. However, it always increases with the growth of the number of fine-tuned blocks on the 10-split DomainNet. The reason is that the split DomainNet is a cross-domain CIL benchmark with various domains and classes. As the capacity of the model increases, the accuracy can improve steadily due to the better adaptation to data. Since the size of the CIFAR-100 dataset is small and the domains vary little, the model is easy to overfit to it and thus causes slight performance degradation.

Nonetheless, the forgetting can almost keep unchanged or decrease as the number of fine-tuned blocks increases. It demonstrates that the proposed Mamba-CL can effectively prevent forgetting in each fine-tuned Mamba block. Given that when all the blocks are fine-tuned, the model can reach the peak accuracy on the DomainNet, and generally achieve satisfied performances on the ImageNet-R and CIFAR100, we uniformly fine-tune all the Mamba blocks in our experiments.

C.4. Analysis of Memory

We analyze the additional memory required by the proposed null-space projections for SSMs as follows. The introduced uncentered covariance matrices (*i.e.*, $\bar{\mathbf{X}}_t \bar{\mathbf{X}}_t^\top \in \mathbb{R}^{D \times D}$, $\bar{\delta}_t \bar{\delta}_t^\top \in \mathbb{R}^{L \times L}$, $\bar{\delta}_t \bar{\mathbf{X}}_t \bar{\delta}_t \bar{\mathbf{X}}_t^\top \in \mathbb{R}^{D \times D}$) and the orthogonal projection matrices (*i.e.*, $\mathbf{H}_1 \in \mathbb{R}^{D \times D}$, $\mathbf{H}_2 \in \mathbb{R}^{L \times L}$, $\mathbf{H}_3 \in \mathbb{R}^{D \times D}$) need to be stored for calculating and performing orthogonal projections during training. Therefore, the additional memory for a total of S layers is formulated as:

$$\text{AdditionalMemory} = 2S(2D^2 + L^2). \quad (27)$$

In our default setting, $D = 2048$, $L = 145$ and $S = 48$. The total additional memory required is approximately 807.36 million floating-point values, which is acceptable since the storage cost is cheap for modern hardware. Note

Table 7. Running time (in minutes) of Mamba-Seq and Mamba-CL on four benchmarks.

| Model | 10S-ImageNet-R | 20S-ImageNet-R | 10S-CIFAR-100 | 10S-DomainNet | Average |
|-----------|----------------|----------------|---------------|---------------|-----------|
| Mamba-Seq | 368 | 412 | 715 | 678 | 543 |
| Mamba-CL | 384 | 433 | 755 | 751 | 581 |
| Increase | 16 (4.3%) | 21 (5.1%) | 40 (5.6%) | 73 (10.8%) | 38 (7.0%) |

that this additional memory is constant and does not increase with the number of tasks or classes, providing an advantage in practical applications compared to those approaches requiring to expand networks or store samples for rehearsal.

C.5. Analysis of Complexity

The additional complexity brought by the null-space projections within a block mainly contains the following parts.

1) The null-space projections in each optimization step. For the gradient matrices \mathbf{G}^δ , \mathbf{G}^C , \mathbf{G}^A and \mathbf{G}^B which are multiplied by \mathbf{H}_1 , \mathbf{H}_1 , \mathbf{H}_2 and \mathbf{H}_3 , respectively, the complexity of matrix multiplication is $\mathcal{O}(D(2DN + LN + D))$. The batch size and epochs are represented as n_{batch} and n_{epoch} , respectively. We denote the total number of samples in each task as M , and there are T tasks. After training all the tasks, the complexity introduced by the null-space projections is $\mathcal{O}(\frac{n_{epoch}MTD(2DN+LN+D)}{n_{batch}})$.

2) The forward process to obtain the intermediate features which will be used for computing uncentered covariance matrices. We denote the computational cost of the model’s forward propagation as C_{model} . Thereby, the introduced additional computation is $MT C_{model}$.

3) Computation of uncentered covariance matrices in each task. The complexity of computing the uncentered covariance matrices is $\mathcal{O}(2TMLD^2 + TM^2L^2)$.

4) Computation of SVD and projection matrices. As the specific complexity of SVD is hard to determine, we use $\mathcal{O}(C_{SVD})$ to represent its complexity for on task. Moreover, the complexity of computing projection matrices derived from the null-space bases is also hard to determine since the number of bases is calculated adaptively. For simplicity, we use $\mathcal{O}(C_{bases})$ to represent the complexity of computing projection matrices. The complexity of these two operations on all the tasks is denoted as $\mathcal{O}(T(C_{SVD} + C_{bases}))$. However, it is worth noting that the SVD, computation of projection matrices as well as the uncentered covariance matrices are only performed once in each task. Therefore, the computational complexity is negligible compared to the whole training process.

Overall, the additional complexity of the proposed approach is $\mathcal{O}(MT[\frac{n_{epoch}}{n_{batch}}D(2DN + LN + D) + (2LD^2 + ML^2) + C_{model}] + T(C_{SVD} + C_{bases}))$.

C.6. Running Time

We report the average running time over three runs for our Mamba-CL and the baseline Mamba-Seq across the four benchmarks, as shown in Table 7. Compared to the baseline Mamba-Seq, the running time of Mamba-CL increases by 16~73 minutes (4.3%~10.8%) across these benchmarks, with an average increase of 38 minutes (7.0%). The additional running time introduced by nulls-space projections is acceptable as it constitutes only a small portion of the overall running time.